RESEARCH ARTICLE | MARCH 04 2024

Impact of Se concentration and distribution on topological transition in FeTe₁-xSe₂ crystals *⊗*

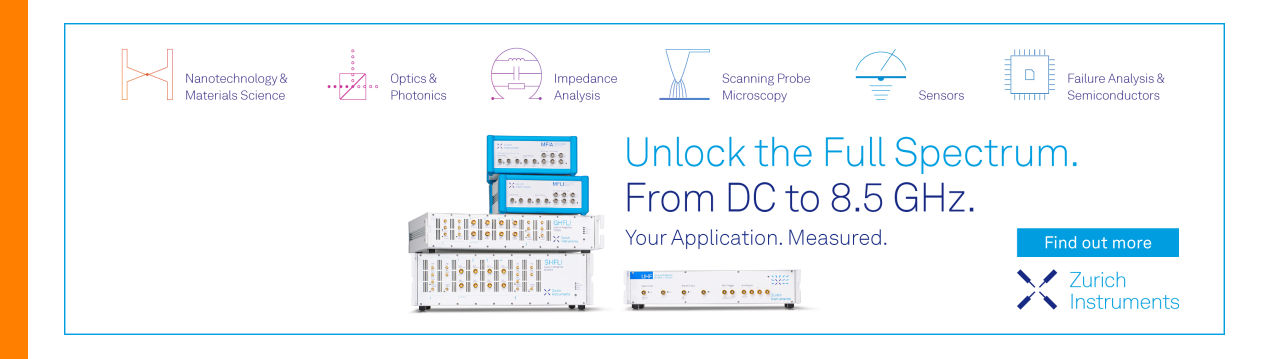
Jinying Wang ■ (i); Gerhard Klimeck ■ (ii)



Appl. Phys. Lett. 124, 103101 (2024) https://doi.org/10.1063/5.0195271









Impact of Se concentration and distribution on topological transition in FeTe_{1-x}Se_x crystals

Cite as: Appl. Phys. Lett. **124**, 103101 (2024); doi: 10.1063/5.0195271 Submitted: 1 January 2024 · Accepted: 17 February 2024 · Published Online: 4 March 2024









Jinying Wang^{1,a)} (D) and Gerhard Klimeck^{1,2,a)} (D)



AFFILIATIONS

- Network for Computational Nanotechnology, Purdue University, West Lafayette, Indiana 47907, USA
- School of Electrical and Computer Engineering, Purdue University, West Lafayette, Indiana 47907, USA

ABSTRACT

A topological phase transition in high-temperature superconductor $FeTe_{1-x}Se_{xy}$ occurring at a critical range of Se concentration x, underlies their intrinsic topological superconductivity and emergence of Majorana states within vortices. However, how Se concentration and distribution determine the electronic states, particularly the presence or absence of Majorana states, in $FeTe_{1-x}Se_x$ remains unclear. In this study, we combine density functional theory calculations with p_z - $d_{xz/yz}$ -based analysis and Wannier-based Hamiltonian analysis to systematically explore the electronic structures of diverse $FeTe_{1-x}Se_x$ compositions. Our investigation reveals a nonlinear variation of the spin-orbit coupling (SOC) gap between p_z and $d_{xz/yz}$ bands in response to the Se concentration x, with the maximum gap occurring at x = 0.5. The $p_z - p_z$ and $d_{x2-y2}-p_z$ interactions are found to be critical for pd band inversion. Furthermore, the distribution of Se significantly modulates the SOC gap, thereby influencing the emergence of Majorana states within local vortices.

Published under an exclusive license by AIP Publishing. https://doi.org/10.1063/5.0195271

The iron chalcogenide family $(Fe_{1+y}Te_{1-x}Se_x)$ has emerged as an intriguing platform to study unconventional superconductivity and quantum state transitions. 1-3 In particular, the recent discovery of topological superconductivity and Majorana bound states (MBS) in FeTe_{0.55}Se_{0.45} has obtained immense attention for its potential in topological quantum computing. The unique electronic properties of this system have been suggested to depend strongly on the Fe and Te/Se concentrations both theoretically $^{6.7}$ and experimentally. In contrast to the topologically trivial FeSe, FeTe_{1-x}Se_x (x = 0.5 in first-principles calculations and x = 0.45 in experiments exhibits nontrivial topological surface states (TSS). These TSS are attributed to the parity inversion and spin-orbit coupling (SOC) gap opening of p and d bands along the Γ to Z path in the Brillouin zone, induced by Te substitution. The sensitivity of topology in iron chalcogenide to the chemical composition is also supported by recent angle resolved photoemission spectroscopy (ARPES) measurements.8 As TSS appears only at a sufficiently high Te concentration, FeTe_{0.55}Se_{0.45} is located near the phase boundaries among nonsuperconducting, normal superconducting, and topological superconducting (TSC) phases.8 The coexistence of TSS and superconductivity gives rise to MBS in vortices, which can be detected using scanning tunneling microscopy (STM) and spectroscopy. 4,5 However, not all vortices host MBS.9 The reasons behind the presence/absence of MBS have been intensely debated, including vortex overlap, vortex disorder, to

Zeeman coupling, 11 and local composition fluctuations. 12 Based on an effective Hamiltonian analysis, Sau et al. 12 have revealed that local fluctuations in Se concentration lead to chemical potential disorders as well as topological domain disorders, thus influencing the presence of MBS. Additionally, local composition fluctuations induce local strains, resulting in nematic transitions and nanoscale suppression of superconductivity in $FeTe_{1-x}Se_{x}^{-13}$ Despite previous studies highlighting the significance of Se concentration for TSS and MBS, the underlying physics about how Se concentration and distribution determine the electronic states remains unsettled.

Exploring the chemical composition effect on the electronic states of FeTe_{1-x}Se_x poses considerable experimental and theoretical challenges. High-quality growth of FeTe_{1-x}Se_x crystals with precise composition control remains experimentally challenging. The physical atomic structure of $FeTe_{1-x}Se_x$ is expected to strongly influence the electronic structure. However, the atomic structure is highly sensitive to the Se/Te concentration and limited reported. 8,14,15 The presence of local disorders further complicates the situation.8 Although a density functional theory (DFT) can offer qualitatively correct explanations of electronic states for certain compositions (e.g., x = 0, 0.5, 1), its failure to accurately describe strong correlation and coupling effects leads to large band renormalization factors when compared to angle-resolved photoemission spectroscopy (ARPES) data. Additionally, these band

^{a)}Authors to whom correspondence should be addressed: wang4205@purdue.edu and gekco@purdue.edu

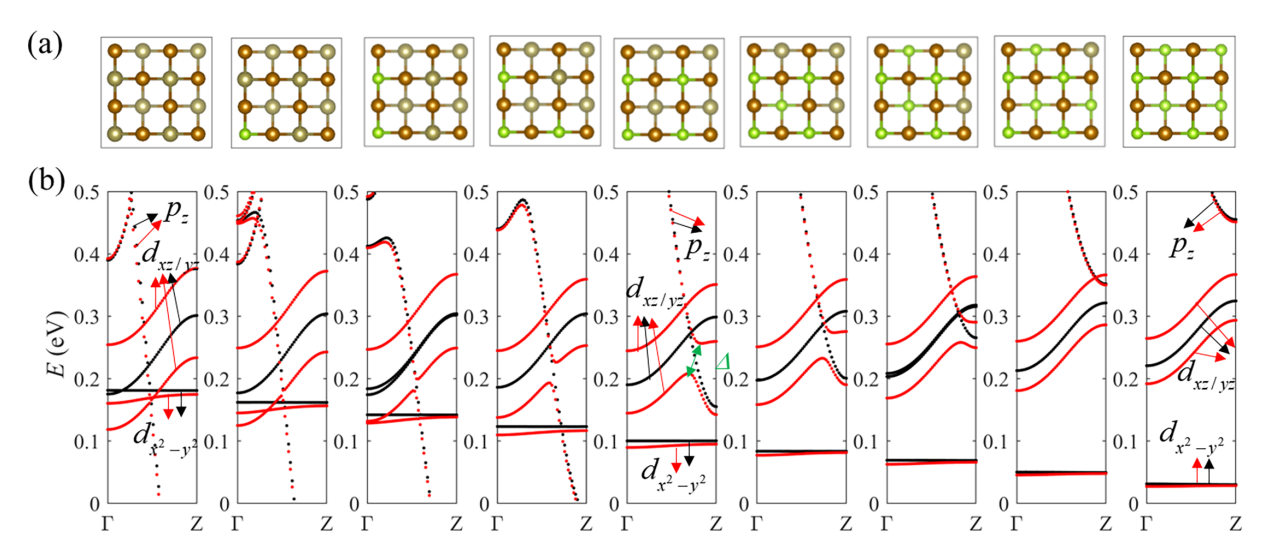


FIG. 1. (a) Atomic structures and (b) band structures of $FeTe_{1-x}Se_x$ (x=0.0, 0.125, 0.25, 0.375, 0.5, 0.625, 0.75, 0.875, and 1.0) calculated by DFT implemented in VASP with (red dot) and without (black dot) SOC effect. The approximated linear relation between lattice constants and x for $FeSe_xTe_{1-x}$ based on experimental data is used, that is, a=7.6406-0.108x (Å) and c=6.3362-0.762x (Å). Atomic positions are optimized using revised Perdew–Burke–Ernzerhof functional. The nonlocal vdW-DF functional.

renormalization factors are dependent on the composition and orbital characteristics. Alternative methods, such as DFT + U and dynamical mean-field theory (DMFT), can improve the renormalization, but they still fail to reproduce the experimental band values. Effective Hamiltonian studies aminly rely on experimental or first-principles results and lack a direct correlation between composition and Hamiltonian terms. Currently, our understanding of the composition effect on orbital interactions and electronic states in $FeTe_{1-x}Se_x$ with varying x is deficient even at a qualitative level, let alone achieving an accurate quantitative description.

Here, we focus on studying the relation among chemical composition, orbital interaction, and electronic structures in $FeTe_{1-x}Se_x$ crystals. By combining DFT calculations, Wannier-based tight-binding (TB) model, and a p_z - $d_{xz/yz}$ -based effective Hamiltonian analysis together, we systematically study the chemical composition effect on electronic states of $FeTe_{1-x}Se_x$, especially the band variation along Γ -Z around Fermi level. The dependence of orbital interaction with x is clarified, and the p_z - p_z and d_{x2-y2} - p_z interactions are found to be critical for pd band inversion.

The variation of Se concentration x in $FeTe_{1-x}Se_x$ crystals changes not only the Se/Te proportion but also the associated atomic structures. The reports on structures of FeTe_{1-x}Se_x are limited and slightly vary with preparation and measurement methods. 19-22 The lattice constants a and c in $FeTe_{1-x}Se_x$ gradually decrease by about \sim 0.05 Å (\sim 2%) and \sim 0.76 Å (\sim 12%), respectively, when x increases from 0 to 1. The relation between a/c and x is approximately linear.²² The bond lengths between Fe and Se/Te atoms or heights between Fe and Se/Te planes (d_z) are rarely reported, 7,21 and the d_z -x relation appears nonlinear. In addition, an uneven local distribution of Se/Te atoms generally exists in $FeTe_{1-x}Se_x$. These pose challenges to determining the accurate atomic structure of $FeTe_{1-x}Se_x$. In this study, we mainly focus on small ordered supercells with fixed concentrations. We study the average composition effect on band structures of $FeTe_{1-x}Se_x$ [x = 0.0, 0.125, 0.25, 0.375, 0.5, 0.625, 0.75, 0.875, and 1.0;Fig. 1(a)] systems using $2 \times 2 \times 1$ supercells of the primitive FeTe_{0.5}Se_{0.5} crystal structure.⁷ As the electronic structures of FeTe_{1-x}Se_x are quite sensitive to both Se/Te proportion and crystal structures, we adopt an experiment-based linear variation of lattice constants with Se concentrations: a = 7.6406 - 0.108x (Å) and c = 6.3362 - 0.762x (Å) and subsequently optimize the atomic geometry using DFT calculations implemented in VASP.

Standard DFT-generalized gradient approximation (GGA) has known limitations in regard to neglecting electron correlation and underestimation of bandgap. Although DMFT and other beyond DFT methods give a better description of correlation and coupling effects, all these calculations show x-dependent and orbital-dependent band renormalization compared to ARPES data. Instead of seeking out the most accurate band calculations, we focus on studying the critical orbital interactions caused by x changes by combining DFT calculations, Wannier TB, and a p_z - $d_{xz/yz}$ -based Hamiltonian analysis together. DFT calculations with GGA-Perdew-Burke-Ernzerhof (PBE)²³ functionals implemented in VASP^{24,25} are used to study the electronic structures of FeTe_{1-x}Se_x crystals. Van-der Waals interactions are included in the optimization of $FeTe_{1-x}Se_x$ systems by using vdW-DF functional.^{26,27} The cutoff energy is set to be 400 eV, and $(7 \times 7 \times 15)$ Monkhorst–Pack grids are used. We set the Fermi level to be zero in all cases. TB Hamiltonians based on maximally localized Wannier functions of FeTe_{1-x}Se_x systems are constructed using Wannier 90. A basis set of five d orbitals $(d_{xy}, d_{xz}, d_{yz}, d_{zz}, and d_{x2-y2})$ of each Fe atom and three p orbitals (p_x, p_y, p_z) of each Se/Te atom is used here. The obtained Wannier functions show the same features to the corresponding atomistic orbitals. A p_z - $d_{xz/yz}$ -based Hamiltonian¹⁶ is used to analyze the band dispersion along Γ -Z direction of $FeTe_{1-x}Se_x$ systems with and without the SOC interaction

$$H(k_z) = \begin{pmatrix} \varepsilon_p + 2t_{pp}\cos k_z & -2\lambda_3\sigma_x\sin k_z & 2\lambda_3\sigma_y\sin k_z \\ & \vdots & \varepsilon_d + 2t_{dd}\cos k_z & i\sigma_z(\lambda_1 + 2\lambda_2\sin k_z) \\ & \vdots & & \vdots \\ & \vdots & & \vdots \\ & & \vdots & & \vdots \end{pmatrix}.$$
(1)

The optimized atomic structures of $FeTe_{1-x}Se_x$ (x = 0.0, 0.125, 0.25,0.375, 0.5, 0.625, 0.75, 0.875, and 1.0, respectively) are shown in Fig. 1(a), where the Fe-Se and Fe-Te bond lengths are 2.34 and 2.51 Å, respectively. The Fe, Se, and Te coordinates remain stable in proximity to their original lattice positions. Neither atomic distortion nor rearrangement is found as the concentration x changes. Figure 1(b) illustrates three distinctive bands near the Fermi level, which are primarily composed of p_z orbitals of chalcogen and $d_{xz/yz}$ and d_{x2-y2} orbitals of Fe according to a projected density of states analysis. The p_z and $d_{xz/yz}$ bands along Γ to Z have shown to be critical for the topology in FeSe_{0.5}Te_{0.5}. As x increases from 0 to 1, the p_z band at Γ exhibits a noticeable upward shift, ultimately leading to the vanishing of band inversion between p_z and $d_{xz/yz}$ bands when x approaches 1. The SOC effect not only causes a split in the degenerate $d_{xz/yz}$ bands but also facilitates hybridization between p_z and $d_{xz/yz}$ bands, thereby opening an SOC gap between them along the Γ -Z path. This SOC gap signifies a topological transition within FeTe_{1-x}Se_x systems, which further leads to the manifestation of topological superconductivity and MBS within vortices at sufficiently low temperatures.4

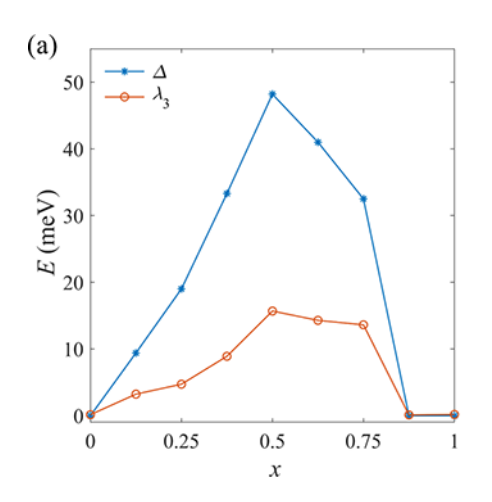
The magnitude of the SOC gap evolves in a nonlinear function of x: it begins at 0.0 meV, reaches its maximum value of $48.2 \,\mathrm{meV}$ at x = 0.5, and subsequently recedes back to 0.0 [see Fig. 2(a)]. This nonlinear variation of SOC gap with x is found to be unaffected by structural optimization methods or lattice structure details. The general behavior apparently hinges solely on the change in the chemical composition (see Figs. S1 and S2 in the supplementary material). To be noted, a larger SOC gap should correspond to more robust MBS.

To understand how the Se concentration affects the orbital interactions and energy bands of FeTe_{1-x}Se_x, we adopt a p_z - $d_{xz/yz}$ -based Hamiltonian¹⁶ as well as a Wannier-based TB approach with a basis set of five d (Fe) and three p (Se/Te) orbitals to fit our DFT results (see Fig. S3 in the supplementary material). The effective pd Hamiltonian reproduces the Γ -Z bands in excellent agreement with DFT results. The onsite and hopping energies, denoted as ε_p , ε_d , t_{pp} , and t_{dd} , mainly control the p and d bands' shape and energy ranges. When x increases from 0 to 1, we observe a gradual increase in both ε_p and ε_d , accompanied by a reduction in t_{pp} and small variation of ε_d and t_{dd} [see Fig. 2(b)]. The inversion of p and d bands along Γ -Z path transpires when the $(\varepsilon_p + 2t_{pp}) - (\varepsilon_d + 2t_{dd})$ and $(\varepsilon_p - 2t_{pp}) - (\varepsilon_d - 2t_{dd})$ terms have opposite signs. The splitting and curvature of $d_{xz/yz}$

bands are predominantly influenced by the $d_{xz}-d_{yz}$ interaction term $i\sigma_z(\lambda_1+2\lambda_2\sin k_z)$ and its conjugate. The $p_z-d_{xz/yz}$ interaction, which is a function of λ_3 , mainly governs the SOC gap between p_z and $d_{xz/yz}$ bands, mirroring a similar trend of variation with the SOC gap itself [see Fig. 2(a)]. In addition, λ_3 ($\lambda_3=15.7$ meV in FeTe_{0.5}Se_{0.5}) in our effective Hamiltonian is comparable to the data fitted to ARPES ($\lambda_3=8$ meV), ¹⁶ making the SOC gap analysis more convincing.

We extend our analysis by employing a Wannier-based TB approach for $FeTe_{1-x}Se_x$ (x = 0, 0.5, and 1) systems to elucidate the intricate correlation between Se concentration and atomic orbital interactions. The fitted Wannier Hamiltonian shows a good description of DFT data (see Fig. S4 in the supplementary material), and the main interaction parameters governing the p_z , $d_{xz/yz}$, and d_{x2-y2} bands are listed in Table I. Some Wannier-based Hamiltonian parameters exhibit variations consistent with those revealed through effective pd Hamiltonian analysis. For example, the on-site energies of d orbitals $(\varepsilon_{d_{xz/yz}}, \varepsilon_{d_{x^2-x^2}})$ vary little with x, while the p-p hopping energies $(t_{pz\sim pz}^0, t_{pz\sim pz}^0)$ $t_{pz \sim pz}^1$) decline as x increases. This observation mirrors the inherent stability of Fe lattices under varying x and the greater localization of p orbitals in Se compared to Te. The Wannier analysis reveals that the interaction between p_z and d_{x2-y2} is critical for p_z - $d_{xz/yz}$ band inversion, which is ignored in the effective pd Hamiltonian. A stepwise substitution of Wannier Hamiltonian parameters from x = 1 with those from x = 0 (see Fig. S5 in the supplementary material) vividly demonstrates that even a slight reduction in $|t_{dx^2-y^2\sim p_z}|$ triggers a significant descending of p_z band. Consequently, the initially separate p_z and $d_{xz/yz}$ bands intersect and undergo a band inversion. Although other Hamiltonian parameters change with x, their impact on p_z - $d_{xz/yz}$ band inversion remains modest, except for the intralayer p_z - p_z interaction $t_{pz\sim pz}^0$, which not only shifts the p_z band to lower energy range but also broadens it. In summary, $|t_{dx^2-y^2\sim p_z}|$ and $t_{pz\sim pz}^0$ emerge as the most important orbital interactions, which mainly determines the occurrence of pd band inversion. In contrast to the evident impact of p_z - $d_{xz/yz}$ interactions on SOC gap in Eq. (1), multiple interactions encompassing p_z and d orbitals contribute to the SOC gap in Wannier Hamiltonian. Nonetheless, it remains uncertain how these interactions are influenced by x and subsequently govern the SOC gap from the point of the Wannier-based atomistic-orbital perspective.

The above discussion about the impact of Se concentration on the electronic structure of $FeTe_{1-x}Se_x$ is based on specific periodic



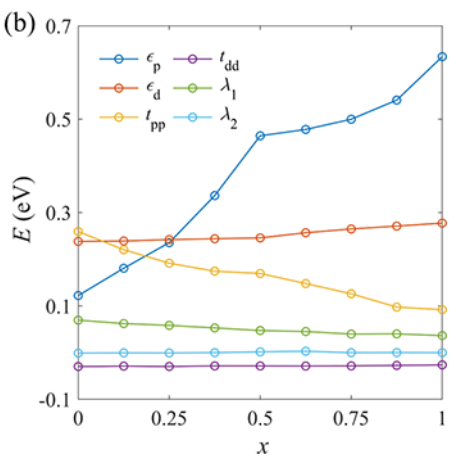


FIG. 2. (a) DFT calculated SOC gap Δ and fitted λ_3 in effective pd Hamiltonian. (b) Remaining pd Hamiltonian parameters of FeTe_{1-x}Se_x (x=0.0, 0.125, 0.25, 0.375, 0.5, 0.625, 0.75, 0.875, and 1.0).

TABLE I. Hamiltonian parameters in Wannier-functions-based Hamiltonians for FeSe_xTe_{1-x} (x = 0.0, 0.5, and 1.0) systems without and with SOC effect. The on-site energies of $d_{xz/yz}$, d_{xz-yz} orbitals of Fe and p_z orbitals of chalcogen are noted as $\varepsilon_{d_{xz/yz}}$, ε_{d_zz-yz} , and $\varepsilon_{p_z(Se,Te)}$, respectively. Also, $t_{p_z(Se,Te)-d_{xz/yz}}$, $t_{p_z(Se,Te)-d_{xz/yz}}$, and $t_{p_z-p_z}^1$ are the hopping energies of nearest-neighbor p_z - d_{xz-yz} , p_z - $d_{xz/yz}$, intralayer p_z - p_z , and interlayer p_z - p_z interaction terms, respectively. Fermi energy is set to zero.

	x	0.0	0.5	1.0
$H_{ m W90}$ woSOC	ε _{dxz/yz} (eV)	-0.694	-0.733, -0.651	-0.688
	$\varepsilon_{\mathrm{dx2-y2}}$ (eV)	-0.721	-0.745	-0.779
	$\varepsilon_{\mathrm{pz(Se, Te)}}\left(\mathrm{eV}\right)$	-2.758	-3.053, -2.679	-2.976
	$ t^{0}_{pz(Se, Te)-dx2-y2} $ (eV)	0.549	0.608, 0.640	0.672
	$ t^0_{\text{pz(Se,Te)}-\text{dxz/yz}} $ (eV)	0.196	0.237, 0.092	0.164
	$t^0_{\mathrm{pz-pz}}$ (eV)	0.268	0.224	0.186
	t^{1}_{pz-pz} (eV)	0.322	0.318	0.302
$H_{ m W90}$ wSOC	$\varepsilon_{ m dxz/yz}$ (eV)	-0.720	-0.717, -0.631	-0.713
	$\varepsilon_{\mathrm{dx2-y2}}$ (eV)	-0.786	-0.773	-0.848
	$\varepsilon_{\rm pz(Se, Te)}$ (eV)	-2.778	-3.083, -2.728	-2.990
	$ t^{0}_{pz(Se, Te)-dx2-y2} $ (eV)	0.548	0.606, 0.640	0.694
	$ t^0_{\text{pz(Se,Te)}-\text{dxz/yz}} $ (eV)	0.196	0.238, 0.092	0.143
	$t_{\text{pz-pz}}^{0}\left(\text{eV}\right)$	0.267	0.223	0.186
	$t^{1}_{\text{pz-pz}}^{1}$ (eV)	0.322	0.318	0.303

structures for each x value which maximize the dispersion of Se and Te atoms. However, real samples manifest uneven distributions of Se and Te atoms. For instance, STM mappings have indicated that the fluctuations in local Se concentration on surfaces surpass 10%. To address the variability in the distributions of Se atoms, we first undertake calculations for FeTe_{0.5}Se_{0.5} using differing atomic configurations achieved by modifying the positions of Se/Te within a 2×2 supercell. As shown in Fig. 3, FeTe_{0.5}Se_{0.5} with different Se

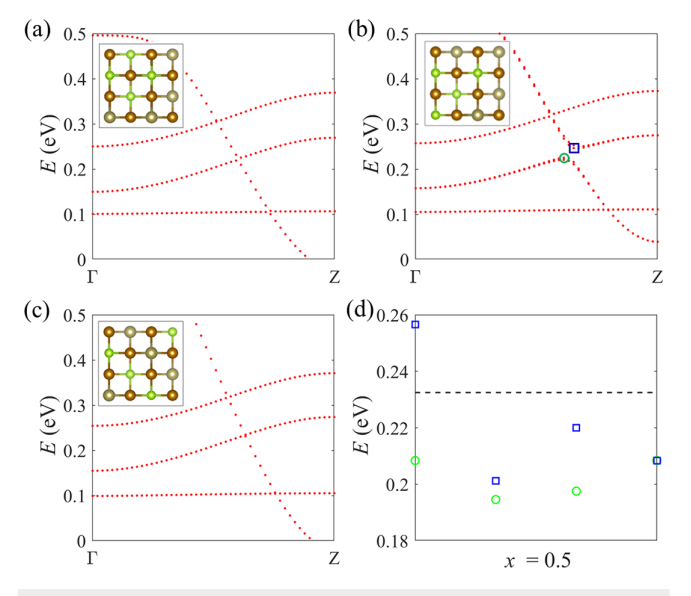


FIG. 3. (a)–(c) Band structures of FeTe_{0.5}Se_{0.5} with three different types of Se/Te atomic distribution. Insets are top views of the atomic structures. (d) The two energy points which determine SOC gap (blue square and green circle) for all four distinct atomic configurations of FeTe_{0.5}Se_{0.5}, and the chemical potential is marked as black dashed line.

distributions exhibits completely distinct electronic structures, with their SOC gaps ranging from 0.0 to 48.2 meV. Especially, the structure in Fig. 3(c) shows a SOC gap of 0 meV. Due to the overlapping of surface states and bulk states, this structure is topologically trivial, making the formation of MBS within vortices nearly implausible. Furthermore, we observe variations in the energy levels of SOC gap within FeTe_{0.5}Se_{0.5} across different atomic distributions. Considering diverse local domains corresponding to these four atomic configurations [Fig. 1(a) and Figs. 3(a)-3(c)] and placing the chemical potential at the dashed line in Fig. 3(d), it becomes apparent that only the local domain resembling the first atomic distribution [as seen in Fig. 1(a) with x = 0.5] is primed for a surface phase transition toward topological superconductivity and the consequent formation of robust MBS, as the chemical potential locates in the SOC gap. ¹⁸ In contrast, the formation of MBS in the other domains is hindered by the substantial occupation of bulk states and the presence of topologically trivial surfaces, attributed to the chemical potential residing well above the SOC gap. Our calculation unveils that the uneven dispersion of Se/ Te atoms leads to fluctuations in both SOC gap and chemical potential of local domains. These fluctuations partly account for the presence and absence of MBS in vortices.

We further explore the electronic properties of the $\mathrm{FeSe}_x\mathrm{Te}_{1-x}$ across varying Se concentrations and distributions. The SOC gap exhibits a nonlinear and intricate behavior as x changes (Fig. 4). As the local disorder of Se increases, it can be expected that both SOC gap and its energy levels in local domains fluctuate. Considering the strong correlation between the SOC gap and chemical potential window for TSC phase in $\mathrm{FeSe}_x\mathrm{Te}_{1-x}$ MBS tends to diminish as the SOC gap contracts. Previous studies have shown the influence of chemical composition on chemical potential and band inversion in $\mathrm{FeSe}_x\mathrm{Te}_{1-x}$ systems.^{7,12,18} For instances, Sau *et al.* have emphasized the distinctive features between topological disorder arising from band inversion and chemical potential disorder, as well as their impacts on the emergence of MBS when Se concentration changes.¹² However, our discovery of

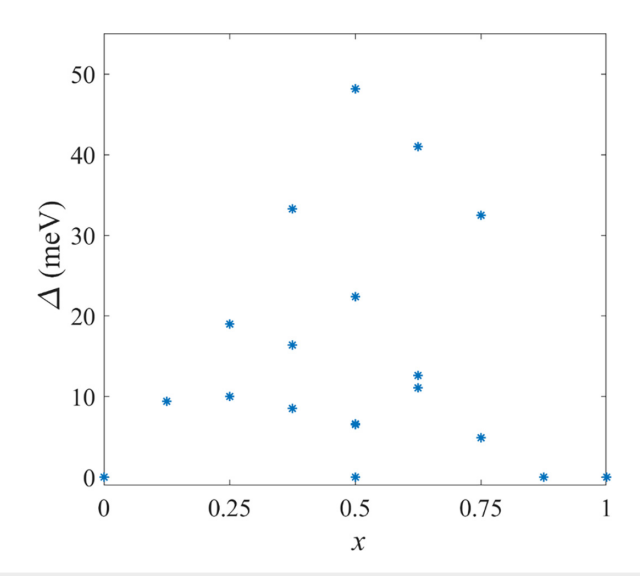


FIG. 4. SOC gap of FeTe_{1-x}Se_x (x = 0.0, 0.125, 0.25, 0.375, 0.5, 0.625, 0.75, 0.875, 1.0) with different Se distributions.

the nonlinear relation between SOC gap and Se concentration/distribution offers a perspective to explain the appearance and disappearance of MBS in localized vortices. The TSC phase and local MBS appears only when the chemical potential aligns within the local SOC gap; otherwise, the localized domains revert to a topologically trivial state.

To be noted, the presence of MBS relies on the simultaneous existence of superconducting and topological state, i.e., TSC phase. Previous experimental studies^{8,29,30} have explored not only the effects of Se/Te concentration but also the influence of Fe contents. In Fe_{1+v}Te_{1-x}Se_x, magnetism and a non-superconducting state are favored in Fe-rich compositions $(1 + y \ge 1)$ due to enhanced magnetic correlations, with TSC occurring only within the superconducting regime at a sufficiently high Te concentration.^{8,30} Our results align with these experimental findings in several aspects: (1) Emphasis on the importance of pd band inversion: We highlight that pd band inversion is the key to the topological phase transition in $FeTe_{1-x}Se_x$. No band inversion occurs when x is large.²⁹ Furthermore, we demonstrate that $|t_{dx^2-y^2\sim p_z}|$ and $t_{pz\sim pz}^0$ are the most crucial orbital interactions, primarily determining the occurrence of pd band inversion. (2) Identification of TSC phase: The TSC phase is found when the Te concentration is sufficiently high, with the maximum probability of detecting local TSC occurring around $x \approx 0.57$. Our calculations reveal a nonlinear variation of the spin-orbit coupling (SOC) gap, determining the probability of TSS, with the maximum gap occurring at $x \sim 0.5$. Although the critical x for the maximum TSS probability slightly differs, our simulations provide an explanation for the underlying physics. (3) Explanation of inhomogeneity in TSS and MBS: Combining the impact of x on chemical potential, we further explain the experimentally observed inhomogeneity of TSS and MBS^{8,9} from the perspective of a nonlinear and intricate SOC gap variation with Se/Te concentration and distribution.

In conclusion, our study explores the intricate relationship between Se composition and electronic states in $FeTe_{1-x}Se_x$. By combining DFT calculations and Hamiltonian analysis, we uncover a

nonlinear variation of the SOC gap between p_z and $d_{xz/yz}$ bands in response to x as well as the critical role of p_z – p_z and d_{xz-yz} – p_z interactions in pd band inversion. Moreover, we find substantial impact of Se distribution on the SOC gap, subsequently influencing the presence or absence of MBS within local vortices. This study reveals the intricate interplay between chemical composition, electronic structure, and Majorana in FeTe_{1-x}Se_x, providing a fresh perspective to understand the appearance and disappearance of MBS.

See the supplementary material for the band structures of $FeTe_{1-x}Se_x$ using DFT with different optimization methods and lattice structures. The fitting of DFT results by the effective Hamiltonian and Wannier-based Hamiltonian is presented. The impact of various terms in the Wannier Hamiltonian is examined.

This work was funded by the U.S. National Science Foundation (NSF QII-TAQS) under Grant No. 1936246. The authors acknowledge the Rosen Center for Advanced Computing at Purdue University and nanoHUB for the use of their computing resources and technical support. We are also grateful for a helpful discussion with Professor Jay D. Sau, Dr. Tamoghna Barik, Professor Jennifer E. Hoffman, and Benjamin H. November.

AUTHOR DECLARATIONS Conflict of Interest

The authors have no conflicts to disclose.

Author Contributions

Jinying Wang: Conceptualization (equal); Data curation (lead); Formal analysis (equal); Investigation (lead); Methodology (lead); Project administration (equal); Resources (equal); Software (equal); Supervision (equal); Validation (equal); Visualization (lead); Writing – original draft (lead); Writing – review & editing (equal). Gerhard Klimeck: Conceptualization (equal); Data curation (supporting); Formal analysis (equal); Funding acquisition (lead); Investigation (supporting); Methodology (supporting); Project administration (equal); Resources (equal); Software (equal); Supervision (equal); Validation (equal); Visualization (supporting); Writing – original draft (supporting); Writing – review & editing (equal).

DATA AVAILABILITY

The data that support the findings of this study are available from the corresponding authors upon reasonable request.

REFERENCES

¹L. Fanfarillo, "Go for a spin," Nat. Phys. 18, 738-739 (2022).

⁵P. Zhang, K. Yaji, T. Hashimoto, Y. Ota, T. Kondo, K. Okazaki, Z. Wang, J. Wen, G. D. Gu, H. Ding, and S. Shin, "Observation of topological

 $^{^{\}mathbf{2}}$ Y. Liu, T. Wei, G. He, Y. Zhang, Z. Wang, and J. Wang, "Pair density wave state in a monolayer high- T_{c} iron-based superconductor," Nature $\mathbf{618}$, 934–939 (2023).

³R. M. Fernandes, A. I. Coldea, Ĥ. Ding, I. R. Fisher, P. J. Hirschfeld, and G. Kotliar, "Iron pnictides and chalcogenides: A new paradigm for superconductivity," Nature **601**, 35–44 (2022).

⁴D. Wang, L. Kong, P. Fan, H. Chen, S. Zhu, W. Liu, L. Cao, Y. Sun, S. Du, J. Schneeloch, R. Zhong, G. Gu, L. Fu, H. Ding, and H. J. Gao, "Evidence for Majorana bound states in an iron-based superconductor," Science 362, 333–335 (2018).

- superconductivity on the surface of an iron-based superconductor," Science 360, 182-186 (2018).
- ⁶L. C. C. Ambolode, K. Okazaki, M. Horio, H. Suzuki, L. Liu, S. Ideta, T. Yoshida, T. Mikami, T. Kakeshita, S. Uchida, K. Ono, H. Kumigashira, M. Hashimoto, D.-H. Lu, Z.-X. Shen, and A. Fujimori, "Se content x dependence of electron correlation strength in Fe_{1+y}Te_{1-x}Se_x," Phys. Rev. B 92, 035104 (2015).
- ⁷Z. Wang, P. Zhang, G. Xu, L. K. Zeng, H. Miao, X. Xu, T. Qian, H. Weng, P. Richard, A. V. Fedorov, H. Ding, X. Dai, and Z. Fang, "Topological nature of the FeSe_{0.5}Te_{0.5} superconductor," Phys. Rev. B 92, 115119 (2015).
- ⁸Y. Li, N. Zaki, V. O. Garlea, A. T. Savici, D. Fobes, Z. Xu, F. Camino, C. Petrovic, G. Gu, P. D. Johnson, J. M. Tranquada, and I. A. Zaliznyak, "Electronic properties of the bulk and surface states of $Fe_{1+y}Te_{1-x}Se_x$ " Nat. Mater. 20, 1221-1227 (2021).
- ⁹T. Machida, Y. Sun, S. Pyon, S. Takeda, Y. Kohsaka, T. Hanaguri, T. Sasagawa, and T. Tamegai, "Zero-energy vortex bound state in the superconducting topological surface state of Fe(Se,Te)," Nat. Mater. 18, 811-815 (2019).
- ¹⁰C. K. Chiu, T. Machida, Y. Huang, T. Hanaguri, and F. C. Zhang, "Scalable Majorana vortex modes in iron-based superconductors," Sci. Adv. 6, eaay0443
- ¹¹A. Ghazaryan, P. L. S. Lopes, P. Hosur, M. J. Gilbert, and P. Ghaemi, "Effect of Zeeman coupling on the Majorana vortex modes in iron-based topological superconductors," Phys. Rev. B 101, 020504(R) (2020).
- ¹²T. Barik and J. D. Sau, "Signatures of nontopological patches on the surface of topological insulators," Phys. Rev. B 105, 035128 (2022).
- ¹³H. Zhao, H. Li, L. Dong, B. Xu, J. Schneeloch, R. Zhong, M. Fang, G. Gu, J. Harter, S. D. Wilson, Z. Wang, and I. Zeljkovic, "Nematic transition and nanoscale suppression of superconductivity in Fe(Te,Se)," Nat. Phys. 17, 903-908 (2021).
- 14K. Terao, T. Kashiwagi, T. Shizu, R. A. Klemm, and K. Kadowaki, "Superconducting and tetragonal-to-orthorhombic transitions in single crystals of FeSe_{1-x}Te_x ($0 \le x \le 0.61$)," Phys. Rev. B **100**, 224516 (2019).
- 15 K. Nakayama, R. Tsubono, G. N. Phan, F. Nabeshima, N. Shikama, T. Ishikawa, Y. Sakishita, S. Ideta, K. Tanaka, A. Maeda, T. Takahashi, and T. Sato, "Orbital mixing at the onset of high-temperature superconductivity in FeSe_{1-x}Te_x/ CaF₂," Phys. Rev. Res. 3, L012007 (2021).
- ¹⁶H. Lohani, T. Hazra, A. Ribak, Y. Nitzav, H. Fu, B. Yan, M. Randeria, and A. Kanigel, "Band inversion and topology of the bulk electronic structure in FeSe_{0.45}Te_{0.55}," Phys. Rev. B **101**, 245146 (2020).
- ¹⁷M. Aichhorn, S. Biermann, T. Miyake, A. Georges, and M. Imada, "Theoretical evidence for strong correlations and incoherent metallic state in FeSe," Phys. Rev. B 82, 064504 (2010).

- ¹⁸G. Xu, B. Lian, P. Tang, X. L. Qi, and S. C. Zhang, "Topological superconductivity on the surface of Fe-based superconductors," Phys. Rev. Lett. 117, 047001
- ¹⁹B. C. Sales, A. S. Sefat, M. A. McGuire, R. Y. Jin, D. Mandrus, and Y. Mozharivskyj, "Bulk superconductivity at 14 K in single crystals of $Fe_{1+y}Te_xSe_{1-x}$ " Phys. Rev. B **79**, 094521 (2009).
- 20 Y. Mizuguchi, F. Tomioka, S. Tsuda, T. Yamaguchi, and Y. Takano, "Substitution effects on FeSe superconductor," J. Phys. Soc. Jpn. 78, 074712
- ²¹A. Martinelli, A. Palenzona, M. Tropeano, C. Ferdeghini, M. Putti, M. R. Cimberle, T. D. Nguyen, M. Affronte, and C. Ritter, "From antiferromagnetism to superconductivity in $\mathrm{Fe}_{1+y}\mathrm{Te}_{1-x}\mathrm{Se}_x$ (0 $\leq x \leq$ 0.20): A neutron powder diffraction analysis," Phys. Rev. B 1, 094115 (2010).
- ²²Y. Kawasaki, K. Deguchi, S. Demura, T. Watanabe, H. Okazaki, T. Ozaki, T. Yamaguchi, H. Takeya, and Y. Takano, "Phase diagram and oxygen annealing effect of FeTe_{1-x}Se_x iron-based superconductor," Solid State Commun. 152, 1135-1138 (2012).
- $^{\bf 23}$ J. P. Perdew, K. Burke, and M. Ernzerhof, "Generalized gradient approximation made simple," Phys. Rev. Lett. 77, 3865-3868 (1996).
- ²⁴G. Kresse and J. Furthmüller, "Efficient iterative schemes for ab initio totalenergy calculations using a plane-wave basis set," Phys. Rev. B 54, 11169-11186 (1996).
- ²⁵G. Kresse and D. Joubert, "From ultrasoft pseudopotentials to the projector augmented-wave method," Phys. Rev. B **59**, 1758–1775 (1999). ²⁶Y. Zhang and W. Yang, "Comment on 'generalized gradient approximation
- made simple," Phys. Rev. Lett. 80, 890 (1998).
- ²⁷M. Dion, H. Rydberg, E. Schröder, D. C. Langreth, and B. I. Lundqvist, "Van der Waals density functional for general geometries," Phys. Rev. Lett. 92, 246401 (2004).
- ²⁸G. Pizzi, V. Vitale, R. Arita, S. Blügel, F. Freimuth, G. Géranton, M. Gibertini, D. Gresch, C. Johnson, T. Koretsune, J. Ibañez-Azpiroz, H. Lee, J.-M. Lihm, D. Marchand, A. Marrazzo, Y. Mokrousov, J. I. Mustafa, Y. Nohara, Y. Nomura, L. Paulatto, S. Poncé, T. Ponweiser, J. Qiao, F. Thöle, S. S. Tsirkin, M. Wierzbowska, N. Marzari, D. Vanderbilt, I. Souza, A. A. Mostofi, and J. R. Yates, "Wannier90 as a community code: New features and applications," J. Phys.: Condens. Matter 32, 165902 (2020).
- ²⁹X.-L. Peng, Y. Li, X.-X. Wu, H.-B. Deng, X. Shi, W.-H. Fan, M. Li, Y.-B. Huang, T. Qian, P. Richard, J.-P. Hu, S.-H. Pan, H.-Q. Mao, Y.-J. Sun, and H. Ding, "Observation of topological transition in high- T_c superconducting monolayer $FeTe_{1-x}Se_x$ films on $SrTiO_3(001)$," Phys. Rev. B **100**, 155134 (2019).
- 30 J. M. Tranquada, G. Xu, and I. A. Zaliznyak, "Magnetism and superconductivity in $Fe_{1+y}Te_{1-x}Se_x$," J. Phys.: Condens. Matter 32, 374003 (2020).